BMJ Open Ophthalmology

AI-MK: artificial intelligence for assessing and monitoring microbial keratitis

Colby Hart ,[1] Xu Chen,[2,3] Mahmoud Ahmed,[4] Matteo Airaldi,[5] Alfredo Borgia ,[6,7] Daniel Mahini,[8] Tobi Somerville ,[9] Saaeha Rauz,[10,11] Adela Hulpus,[4,12] Vito Romano ,[13] Gibran Butt ,[14] Giulia Coco ,[15] Yalin Zheng ,[4,12] Stephen Kaye[4,12]

To cite: Hart C, Chen X, Ahmed M, *et al*. AI-MK: artificial intelligence for assessing and monitoring microbial keratitis. *BMJ Open Ophthalmology* 2026;**11**:e002556. doi:10.1136/bmjophth-2025-002556

► Additional supplemental material is published online only. To view, please visit the journal online (https://doi.org/10.1136/bmjophth-2025-002556).

CH and XC contributed equally.

CH and XC are joint first authors.

Received 24 October 2025
Accepted 19 December 2025

For numbered affiliations see end of article.

Correspondence to
Professor Saaeha Rauz; s.rauz@bham.ac.uk

ABSTRACT

Background/Aims To evaluate the performance of an artificial intelligence (AI) model for detecting and monitoring microbial keratitis (MK) using anterior segment optical coherence tomography (AS-OCT).

Methods This is a prospective observational study. Patients with clinically suspected MK and healthy participants were included. In addition to routine assessment and treatment with topical fluoroquinolone therapy, patients underwent AS-OCT at each clinic visit. These images were tested on our DeepLabV3 network-based AI model, which aims to diagnose and record changes to infiltrate sizes of MK lesions over time.

Results The AI model accurately captured MK lesions in 93% of cases (152/163). MK was not detected in scans from healthy eyes, and there were no cases of artefact being falsely detected. The model had a sensitivity of 93% (95% CI 88% to 97%), specificity of 100% (95% CI 88% to 100%), positive predictive value of 100% (95% CI 98% to 100%) and negative predictive value of 73% (95% CI 61% to 83%). Using only the corneal component with masking of the anterior chamber, the AI model showed agreement on change with both observers in 76% (13/18) cases.

Conclusions This AI framework reliably identified MK lesions using AS-OCT, with high sensitivity and specificity. The framework was able to identify change in most cases compared with corneal specialists.

WHAT IS ALREADY KNOWN ON THIS TOPIC

⇒ Previous studies have used artificial intelligence (AI) on slit-lamp or external images for microbial keratitis (MK) diagnosis, but none have leveraged anterior segment optical coherence tomography (AS-OCT) for MK detection or monitoring.

WHAT THIS STUDY ADDS

⇒ This study presents the first AI model trained to detect and monitor MK lesions using AS-OCT, achieving high sensitivity and specificity.

HOW THIS STUDY MIGHT AFFECT RESEARCH, PRACTICE OR POLICY

⇒ AI-MK offers a scalable, objective tool to support clinical decision-making in MK, potentially improving patient outcomes through earlier treatment adjustments.

INTRODUCTION

Microbial keratitis (MK) remains a leading cause of blindness. Although the clinical diagnosis of MK can be relatively straightforward, identifying and objectively measuring clinical change can be difficult. Developments in anterior segment optical coherence tomography (AS-OCT) have improved the assessment and measurement of corneal lesions compared with slit-lamp biomicroscopy.[1] Artificial intelligence (AI) plays a significant and increasing role in diagnosing and monitoring conditions in all medical specialties.[2–4] Within ophthalmology, deep learning models have been created that are able to objectively characterise conditions such as cystoid macular oedema,[5] diabetic retinopathy[6] and glaucomatous disc cupping.[7] There are, therefore, many potential benefits from having an automated system that can objectively assess and monitor corneal lesions such as in MK.

One of the limitations of using slit-lamp biomicroscopy to assess disease, such as infiltrate size, is that the assessment is often limited to the anterior component of the lesion. As such, clinicians rely on measuring ulcer and anterior infiltrate size, which may not reflect changes to the posterior extent of the lesions. In contrast, although not all of the lesions may be characterised by AS-OCT, it does enable an increased depth of measurement than apparent on slit-lamp biomicroscopy, so that the extent of the lesion can be better appreciated. This information may help the clinician to better assess response to treatment and whether treatment modification is needed. AS-OCT has become a standard clinical tool; however, it is difficult for the clinician to compute and compare due to the large number of sections in a scan. Manually

measuring lesions on AS-OCT is time-consuming, having to go through multiple radial sections and then comparing change over time periods is challenging. This also introduces potential measurement error. Having a computerised algorithm that can rapidly and objectively measure and compare lesions across multiple scans, particularly to quantify and to determine change, would be potentially helpful in a patient's management. This type of measurement and its compilation and comparison is well suited to AI.

Several deep learning models have been proposed in the past 5 years to assist in the diagnosis of MK. Most of these approaches applied convolutional neural networks (CNNs) to corneal images, often from slit-lamp or external photographs, rather than from OCT scans. For instance, Apushkin *et al* trained five CNN models on handheld camera images to differentiate fungal keratitis from bacterial keratitis.[8] Their best-performing model, MobileNet, achieved an area under curve (AUC) of 0.86, surpassing expert ophthalmologists (combined AUC of 0.84 vs experts' 0.76).[9] Similarly, Li *et al*[7] developed a deep learning system using DenseNet121 to detect keratitis versus other corneal conditions.[10 11] Their model, tested on smartphone images, achieved an AUC of 0.967, with 91.9% sensitivity and 96.9% specificity for identifying keratitis. In a related study, Wang *et al*, explored different image crops and sources: using InceptionV3 on slit-lamp images, they achieved an AUC of 0.9588, while performance dropped to 0.8529 on uncropped smartphone photos.[12] This highlighted the significant impact of image quality and context, where even after preprocessing, mobile images performed poorly, likely due to variations in lighting and focus conditions. Notably, none of these models used OCT scans for training or validation. The aim of this study was to develop an AI model and to evaluate the effectiveness of this model in assessing and monitoring change in MK using AS-OCT.

MATERIALS AND METHODS

The AS-OCT images were initially captured with Cassia (Tomey GmbH, Nuremberg, Germany) and then on Anterion (Heidelberg Engineering GmbH, Heidelberg, Germany) devices. All lesions on the AS-OCT images were traced by two corneal specialists and used as the ground truth to train and evaluate the AI model. Annotation between corneal specialists showed agreement in >98% of images. When agreement was not made between observers, a third corneal specialist (SK) decided on lesion demarcation. Examples of annotations of each class are presented in online supplemental figure 1.

For the initial training phase, our AI model was trained on AS-OCT scans from healthy eyes and patients with corneal lesions due to corneal dystrophies and MK. This was then repeated on patients presenting with clinically suspected MK at presentation and at 1 week, to assess progression. All patients with clinically suspected MK received a topical fluoroquinolone at presentation and treatment modified according to the microbiological diagnosis and clinical response.

The proposed AI segmentation framework consists of two stages: AI-based segmentation and post-processing, as illustrated in online supplemental figure 2. In the AI segmentation stage, we incorporated two deep learning-based segmenters—a global and a local segmenter—to ensure high accuracy in identifying key anatomical structures and disease markers. These segmenters generated initial segmentations of MK regions, which are then refined in the post-processing step to produce the final segmentation result. The framework is described in detail below. It was not deemed appropriate to involve patients or the public in the design or conduct of our research.

AI segmentation stage

Model architectures

The global segmenter was designed as a four-class segmentation model. The primary function of the global segmenter was to filter out general objects or artefacts that might visually resemble the cornea. This process was crucial for ensuring that subsequent segmentation is focused solely on the key anatomical structures relevant to the identification of MK. The segmentation categories included the cornea, iris, optical artefacts and the background. The local segmenter was designed as a three-class segmentation model. This segmenter specifically targeted regions of corneal tissues within the image and classified these corneal regions into three distinct categories: those with a higher likelihood of being an MK infiltrate, those with a lower likelihood of being an MK infiltrate, and those corresponding to non-MK areas. The role of the local segmenter was critical in distinguishing between corneal regions that exhibited characteristics consistent with MK and those that did not.

Both segmenters used the DeepLabV3+ architecture, a widely used CNN design for semantic segmentation problems. DeepLabV3+ was introduced by Polat[13] as an improvement over the earlier DeepLab versions, combining a powerful encoder–decoder structure with Atrous convolutions and spatial pyramid pooling (SPP). Atrous convolutions expand the receptive field without losing resolution, capturing multiscale features, while SPP applies parallel convolutions at different dilation rates to capture context at multiple scales. This architecture is well regarded for its ability to capture rich contextual information at multiple scales and produce finely detailed segmentation masks, making it especially effective for complex images such as medical scans.[14] To improve efficiency and enhance feature extraction capabilities, we incorporated EfficientNet (ref: arXiv:1905.11946) as the pretrained encoder in our model. EfficientNet is known for its highly optimised architecture, which balances depth, width and resolution to achieve superior performance with fewer parameters compared with traditional convolutional networks. By leveraging its prior training on the ImageNet dataset (ref: arXiv:1409.0575), we were able to take advantage of the

robust feature representations learnt during ImageNet training.

Training phases

The loss function employed in this study was a combination of dice loss and cross-entropy loss, both weighted equally to give them equal importance during training. The dice loss was used to measure the overlap between the predicted segmentation mask and the ground truth, emphasising spatial accuracy and smooth segmentation boundaries. The cross-entropy loss penalised the discrepancies between the predicted class probabilities and the true class labels, ensuring the model accurately classifies each pixel. The balanced combination of these two loss functions helped the model achieve both precise segmentation and accurate classification. For optimisation, the Adam optimiser was chosen due to its adaptive learning rate and efficient gradient computation. The Adam optimiser is particularly effective for deep learning models, as it dynamically adjusts the learning rate during training, which helps avoid overshooting the optimal parameters and facilitates faster convergence. The initial learning rate was set to 0.001, a standard starting point, and this learning rate remained fixed during the early stages of training. The learning rate decay strategy used in this study reduced the learning rate by a factor of 0.9 after every five epochs to help the model fine-tune the weights as it converged. To enhance the robustness and generalisation capability of the segmenters, a series of data augmentation techniques were employed. These augmentation methods included image flipping, random rotation, random brightness adjustment and random contrast adjustment. By applying these transformations, we generated multiple variations of the input images, thereby increasing the diversity of the training data. This strategy exposed the models to a wider range of variations and potential scenarios, improving their ability to generalise and perform well on unseen data. Any discrepancy in tracing of corneal lesions by the two observers in the training phase was settled by the principal author.

Inference phases

During the inference phase, a new image for the analysis is processed through both the well-trained global and local segmenter in parallel to produce initial segmentation maps. The output from the global segmenter provides an initial segmentation of the image into regions such as the cornea, iris branches and background. The output from the local segmenter refines the corneal region identified by the global segmenter, classifying it into categories based on the likelihood of being affected by MK. After obtaining the outputs from both segmenters, logical operations are applied to combine the segmentation results into an initial segmentation map subject to the post-processing step.

Post-processing

The post-processing step addresses the significant challenge due to the inherent similarity in texture between the sclerocorneal junction area and the MK infiltrate region. This similarity led to the generation of false positives, particularly within normal frames, where the MK infiltrate was misidentified. To address this issue, we developed a multistep post-processing approach. First, we applied iris corner detection, identifying the key corners of the iris as central reference points. In parallel, a fixed radius setting was implemented, establishing a predetermined radius for consistent reference points. Using this setup, we applied circular masking to eliminate false MK infiltrate segmentation within these circles, ensuring that only relevant MK infiltrate regions were retained (online supplemental figure 3). This step effectively removed unwanted segmentation, improving the precision of the final analysis. However, our experimentation revealed a limitation in the effectiveness of fixed circles, particularly when applied to real-world images. The fixed radius approach struggled to adequately exclude junction areas, as the dynamic nature of iris positioning meant that the irises did not consistently align horizontally. This misalignment resulted in inadequate coverage of the junction regions by the fixed circles. To overcome this challenge, we introduced a novel method called Adaptive Circles for Exclusion (ACE) (online supplemental figure 3). ACE employs mathematical algorithms to dynamically calculate the optimal radius required to encompass a specified percentage of the area. In practical applications, we determined that setting the radius to cover 15% of the cornea area provided sufficient coverage to account for positional variations in iris alignment. This adaptive approach ensured that the junction areas were consistently included, regardless of the iris's position, enhancing the robustness and effectiveness of the post-processing technique.

Datasets

A total of 656 images from 250 patients with MK and corneal dystrophies (42.46 years (SD 9.12)) were used to train the two AI-based segmenters. The strategy for overfitting and fair comparison employed splicing of the dataset at the patient level for training and testing. The inclusion of corneal dystrophy lesions was to provide lesions distinct from clearly demarcated MK lesions for the algorithm to train on. For training the two AI-based segmenters, we employed a standard training–validation–testing split: training (80%) and testing (20%). To maintain consistency and compatibility across the dataset, all input images were resized to a resolution of 512×512 pixels. Subsequently, the pixel values were normalised to the range of (0, 1), which is a common practice in deep learning to standardise the input data for better model performance.

Test phase

Following the training phase, the sensitivity and specificity of the model were then tested on a new dataset

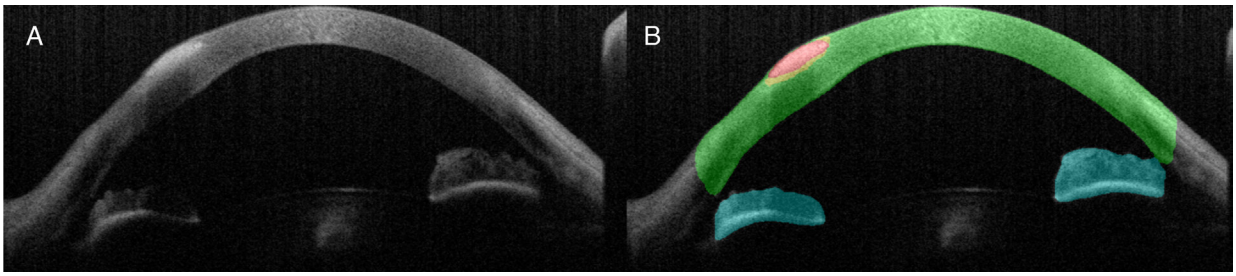

Figure 1 Anterior segment optical coherence tomography (OCT) of an anterior stromal infiltrate. (A) Demonstrates OCT image that was interpreted by the two blinded corneal specialists and (B) demonstrates the AI assessment of higher likelihood (red pixels), lower likelihood (yellow pixels) corneal infiltrates, normal cornea (green pixels) and normal iris (blue pixels).

of 177 Anterion AS-OCT images from 69 patients with MK (53.10 years (SD 18.1)). The images were evaluated and traced by two separate corneal specialists compared with 30 fellow normal eyes with no discernible lesions. Images with gross distortion such as those with perforation and loss of the anterior chamber were excluded (n=14), leading to 163 images with MK lesions for the final analysis. An area of exclusion was created near the junction of the iris and cornea. The AI programme then assessed images by first identifying areas of normal cornea (coloured green, figure 1) and iris (coloured blue, figure 1). Areas identified by the AI as having a higher likelihood of being an infiltrate were highlighted with red pixels and areas of lower likelihood generated yellow pixels (figure 1). The same two specialists who had traced and measured the lesions then interpreted the AI-generated images to assess if: the majority of the lesion was captured or the lesion missed, if artefact had been flagged as MK and if lesions were detected in normal eyes.

Change phase

To assess change (either progression or resolution) of MK, Anterion AS-OCT images were collected in 18 patients (online supplemental table 1), on presentation with MK and after 1 week of treatment. For each visit, 15 radial AS-OCT images through the centre of the cornea were entered for assessment by the AI and two corneal specialists. The demarcation of the cornea lesion on all 15 slices was compared between scans by the specialist in the same way that they would view a clinical AS-OCT—by scrolling through the images multiple times, looking at changes to the size and extent of the corneal lesion. This allowed for interpretation of the entire cornea rather than a single AS-OCT slice through the infiltrate, which was difficult to align on sequential images from previous attempts. By providing specialists with access to all 15 slices from the AS-OCT, perfect OCT slice alignment was not required as would be the case with comparing single OCT slices. The anterior chamber was masked on the images interpreted by the corneal specialists (figure 2), as we found that previous attempts at interpreting the AS-OCT were influenced by changes in inflammation in the anterior chamber, which were not assessed by the AI module. An interval of 1 week between AS-OCT images was chosen as it was considered a sufficient period for measurable change to have occurred clinically and on the AS-OCT. The AI determined that the MK was improving if the sum of the number of pixels (red plus yellow) detected in all 15 OCT slices per visit was reduced compared with the number of pixels from the 15 prior OCT images and worsening if the total number of pixels increased. This was compared with blinded corneal specialist interpretation of the same OCT images.

Performance analysis

Descriptive statistics were applied to calculate specificity, sensitivity, positive and negative predictive values. Positive predictive value represents the probability that the disease is present when the test is positive. Negative predictive value is the probability that the disease was not present when the test is negative.

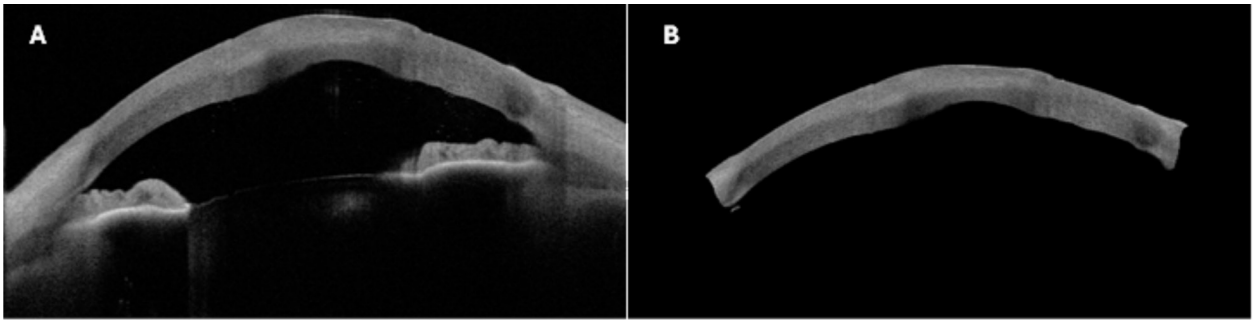

Figure 2 (A) unmasked anterior segment optical coherence tomography (AS-OCT) image and (B) masked AS-OCT image that was interpreted by the blinded observer.

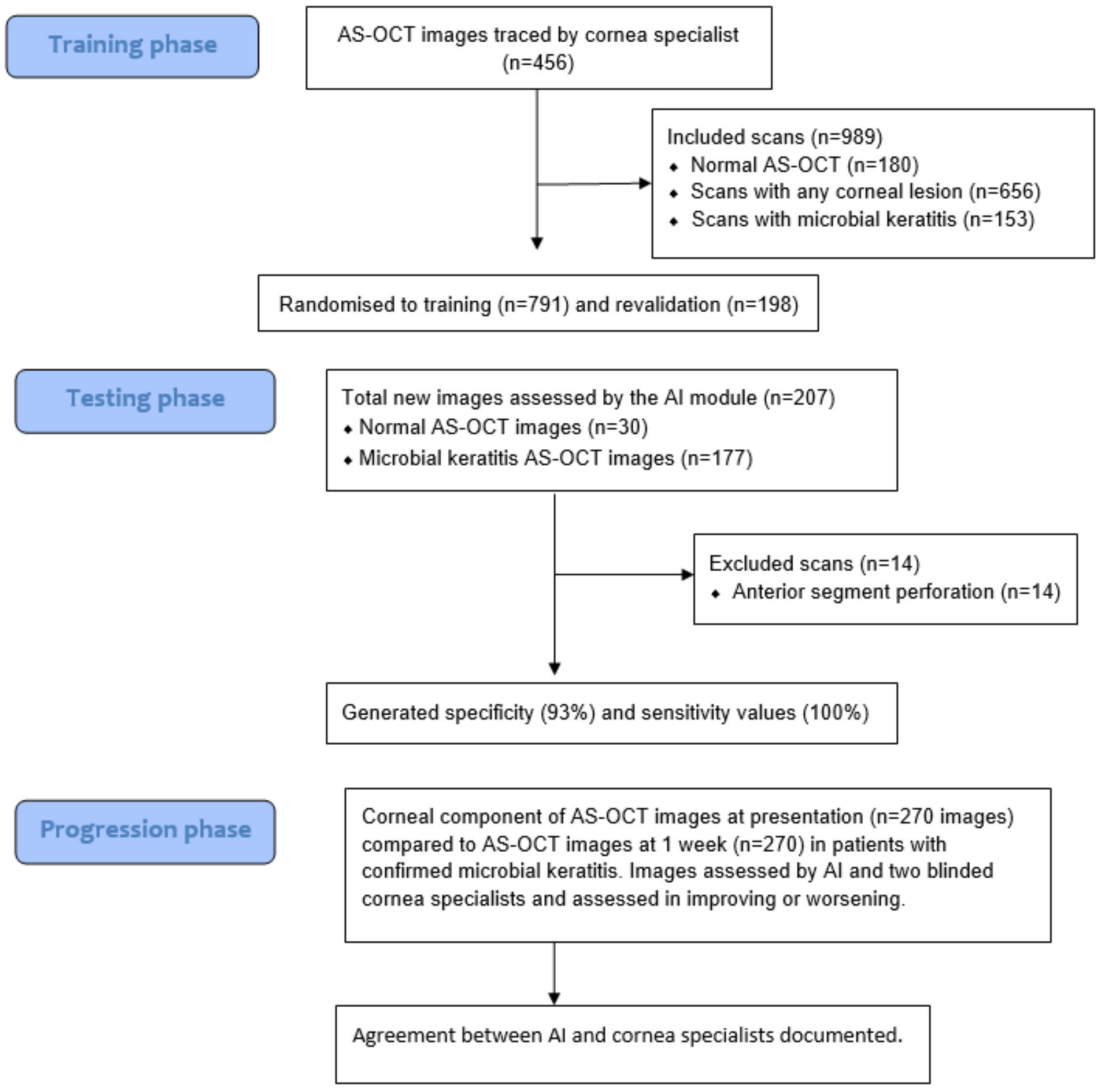

Figure 3 Flow of images used in the training, testing and progression phase of the study. AI, artificial intelligence; AS-OCT, anterior segment optical coherence tomography.

RESULTS

Identification of MK lesions AS-OCT

The AI model accurately captured the majority of the MK lesions (93%, 152/163 cases). The flow of images used in the study is summarised in figure 3 and the demographics, clinical changes and causative organism of the included MK cases are listed in online supplemental table 1. MK was not detected in any AS-OCT scans from the contralateral clinically healthy eyes and there were no cases of artefact being falsely detected by the AI model. MK lesions were missed in 7% (11/163) of images (figure 4). All images of missed infiltrates are included in online supplemental figure 6. These data yielded a sensitivity of detecting MK by our AI software of 93% (95% CI 88% to 97%), the specificity was 100% (95% CI 88% to 100%), the positive predictive value was 100% (95% CI 98% to 100%) and negative predictive value was 73% (95% CI 61% to 83%).

Identification of progression of MK lesions AS-OCT

Using only the corneal component of AS-OCT images, the AI model showed agreement of change with observer 1, 65% of the time (11/18 cases) and observer 2, 76% of the time (13/18 cases). There was agreement between the two specialists in 94% (17/18) of cases (table 1). Online supplemental figure 4 shows images of where there was agreement in the change in MK between AI and an observer and online supplemental figure 5 where there was disagreement.

DISCUSSION

This study evaluated the effectiveness of AI in discerning and measuring corneal lesions in MK and measuring change using AS-OCT. We found that AI is an effective tool in identifying MK using AS-OCT in the majority of cases, with a high sensitivity of 93%. Implementation of our module in hospital clinics could significantly improve the workflow of doctors managing patients with MK.

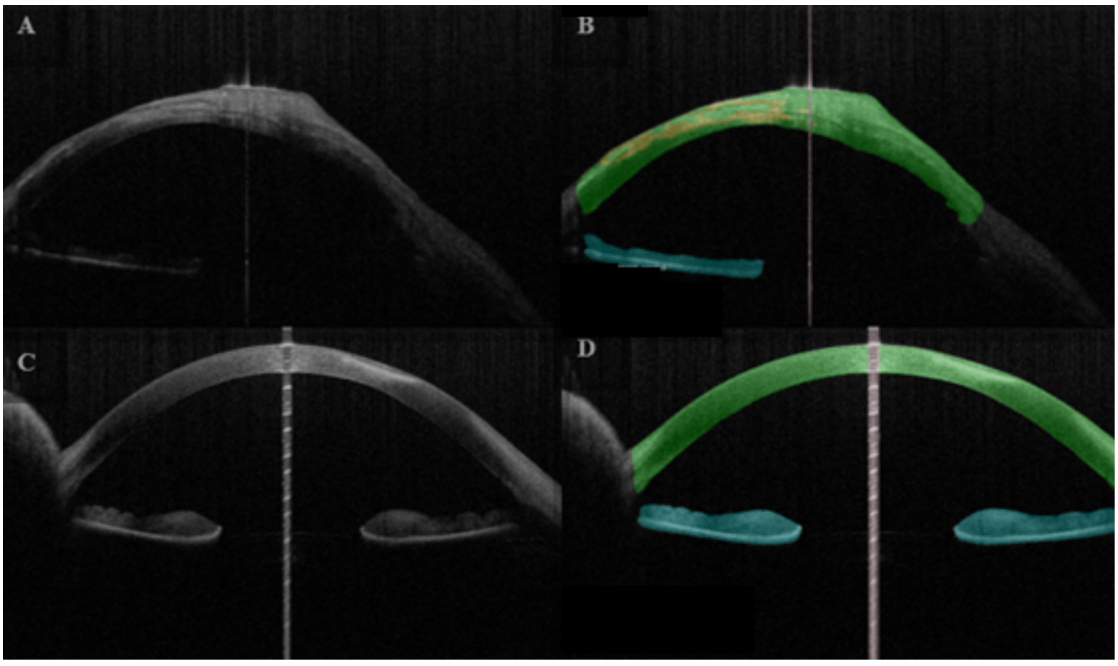

Figure 4 Anterior segment optical coherence tomography of two cases where the artificial intelligence (AI) model failed to identify the microbial keratitis lesions. (A,C) The image entered the AI testing phase. (B,D) The AI interpretation of the image. Note the large infiltrate (B) and small infiltrate (D) that are not detected as abnormal by the AI model.

Integration with commonly used OCT machines may allow the software to rapidly characterise the MK lesion and provide the clinician with an approximate estimate of total size of the infiltrate in three dimensions. The goal would then be able to provide the clinician with a comparison tool for infiltrate size over time, which would be more accurate than traditional measurements of epithelial defect and infiltrate size at the slit lamp. One benefit of the application of our algorithm is that it would reduce interobserver variability on the same lesions, which may be particularly beneficial in clinics where patients are being reviewed by different clinicians at each visit.

Cases that were missed by the AI model were typically small peripheral infiltrates near the limbus. The reason that these cases were missed was due to a mechanism incorporated into the AI model where peripheral abnormalities near the iris are excluded. This was created because, in previous iterations of the model, we were detecting high numbers of artefacts in this anatomical area due to hyperreflectivity at the limbus. Future iterations of the model will aim to reduce the size of this exclusion zone to optimise peripheral lesion detection, while maintaining low false positive rates.

Table 1 Summary of number of images with agreement of progression comparing observer 1 (MAi), observer 2 (MAh) and the AI to the clinical notes

	Observer 1	Observer 2	Clinical notes
AI	76%	76%	53%
Observer 1	n/a	94%	71%
Observer 2	94%	n/a	71%

AI, artificial intelligence.

For the training set, problems arose due to the presence of normal AS-OCT slices in our dataset that did not have an MK infiltrate. Combining normal and abnormal slices into a single segmenter set, however, would lead to an imbalanced training set, as normal slices dominated the other classes. This imbalance can adversely affect the model's ability to learn and accurately classify the minority classes, such as the MK infiltrate regions. Second, we faced a pixel-level imbalanced class problem within the MK infiltrate classes. The regions corresponding to higher and lower likelihoods of being an MK infiltrate were relatively small compared with the overall image space. These smaller regions, however, contained crucial details to help differentiate between different stages or types of MK infiltrates. If, however, we were to have trained a single segmenter for all the classes together, the model might then have struggled to allocate sufficient attention and resources to accurately segment these small regions. This would have led the model to prioritise the larger and more dominant background class, leading to suboptimal performance in segmenting the MK infiltrate classes. By developing two separate segmenters, however, we addressed these imbalanced class challenges more effectively. The global segmenter focused on excluding general objects/artefacts that resembled the cornea and it handled the sample-level imbalanced class problem by distinguishing between the background and the other classes. The local segmenter specifically targeted the MK infiltrate regions and mitigated the pixel-level imbalanced class problem by prioritising the segmentation of these smaller regions. Overall, the decision to develop

two separate segmenters for the total classes was driven by the need to address sample-level and pixel-level imbalanced class problems, ensuring accurate and reliable segmentation results.

During the inference phase, test AS-OCT scans underwent simultaneous processing through both global and local segmenters developed in this study. The goal was to obtain refined segmentation maps by subtracting the segmentation results of the global segmenter from the segmentation results of the local segmenter. This subtraction operation aimed to remove false positive regions that might have been incorrectly classified by the local segmenter. By subtracting the segmentation maps, we focused on the regions that were classified as higher and lower likelihood of being an MK infiltrate by the local segmenter while excluding the general objects/artefacts that resembled the cornea but were not relevant to MK diagnosis. This process helped to refine the segmentation results and enhance the accuracy and reliability of identifying MK infiltrate regions. Other limitations in our study are the absence of MK due to *Acanthamoeba* and other pathogens. Our framework did not evaluate the algorithms' ability to work equally well in bacterial and fungal infections; however, this does represent a gap in our knowledge which could be addressed with a future comparative study.

In summary, our methodology involved the development of two AI-based segmenters and ACE for post-processing. The first global segmenter focused on excluding general objects/artefacts that resemble the cornea, while the second local segmenter aimed to classify regions into higher likelihood MK infiltrates, lower likelihood MK infiltrates, or other non-MK areas. These segmenters could serve as valuable tools for diagnosing MK and monitoring its progression.

A limitation of the model is that it does not have external validation. This is particularly relevant as OCT image characteristics vary based on device and settings. We aimed to address this by including images from multiple OCT devices, but to fully assess the validity of the module, it would require validation on external test sets when these become available. The dataset generated through our research would be made available to any other researcher on request.

The specificity of the AI model for the detection of lesions was perfect and no normal scans were flagged as having MK. This is the result of multiple iterations and deep learning cycles aiming to minimise artefact detection. This does not mean that AI can distinguish MK from other causes of corneal lesions or the type of MK. The current model has been trained not to detect any abnormalities in the anterior chamber, eyelids or at the limbus on the AS-OCT. These areas previously were large sources of artefact error. The tradeoff for this is that some smaller peripheral lesions can be missed. This was a sacrifice that we deemed appropriate, as our goal was to develop an AI software that can be used to track the change of MK lesions based on corneal sections, rather than identify small peripheral infiltrates (which was achieved with high accuracy on previous model iterations).

Although the AI model was effective in detecting MK lesions, the accuracy of which it traced these lesions was limited, as is reflected when looking at the progression (change) in lesions in severe cases. This is evident when there is severe disorganisation of the anterior segment and when treatment also includes wearing contact lenses. We used 656 single-sliced manually traced AS-OCT images to train our AI model, which is fewer than used in deep learning models investigating macular oedema (934 OCT images),[5] diabetic retinopathy (1748 fundus photograph images)[6] and glaucomatous optic neuropathy (48 116 fundus images).[7] As we continue to trace and enter more AS-OCT images of severe cases of MK into the model in the future, we anticipate that the accuracy with which the AI measures corneal lesions in severe cases of MK, that is, those with associated abnormalities in the anterior segment, will improve. Previous studies[5 6] have relied on coding algorithms to enhance the efficiency of image tracing by specialists, which may improve the efficiency of data entry into the deep learning model for clinicians generating similar AI programmes in the future.

The diagnosis of MK is one that is made by the clinician aided by slit-lamp biomicroscopy. The value in AI analysis of MK lesions lies in the ability to detect subtle corneal changes in large lesions that are not easily apparent on slit-lamp examination, which may indicate that the lesion is improving or worsening. This has the potential to help direct treatment or further investigations in such cases. Our study demonstrated that AI can accurately identify change using only corneal sections without anterior chamber or other information in a number (76%) of severe cases compared with specialist OCT interpretation. In this study, we only interpreted corneal changes on the infiltrate, as our AI model was not trained to identify hypopyon size or the presence of anterior chamber cells. Other AI models have shown the ability to quantify the presence of anterior chamber cells[15] and future iterations will aim to also include these factors.

Author affiliations
[1]Cornea, The Royal Victorian Eye and Ear Hospital, East Melbourne, Victoria, Australia
[2]Heart and Lung Research Institute, University of Cambridge, Cambridge, UK
[3]Digital Environment Research Institute, Queen Mary University of London, London, UK
[4]Department of Eye and Vision Science, University of Liverpool, Liverpool, UK
[5]Department of Biomedical and Clinical Science "Luigi Sacco", University of Milan, Milano, Italy
[6]Department of Corneal and External Eye Diseases, Royal Liverpool University Hospital, Liverpool, UK
[7]Department of Biomedical Sciences, Humanitas University, Mexico City, Mexico
[8]The Royal Victorian Eye and Ear Hospital, Melbourne, Victoria, Australia
[9]Department of Eye and Vision Sciences, University of Liverpool, Institute of Ageing and Chronic Disease, Liverpool, UK
[10]Academic Unit of Ophthalmology, University of Birmingham, Birmingham, UK
[11]SWBH NHS Trust, Birmingham and Midland Eye Centre, Birmingham, UK
[12]Royal Liverpool University Hospital, Liverpool, UK

[13]University of Brescia, Brescia, Italy
[14]Academic Unit of Ophthalmology, University of Birmingham College of Medical and Dental Sciences, Birmingham, UK
[15]Ophthalmology, Catholic University, Rome, Italy

Acknowledgements SR acknowledges the UKRI Medical Research Council (MRC – grant code MR/N0199016/1) and the National Institute of Health and Care Research (NIHR – grant code II-LA-1117–2001) and National Institute for Health and Care Research (NIHR) Birmingham Biomedical Research Centre (BRC) for aspects of this work. The views expressed are those of the author(s) and not necessarily those of the UKRI, NIHR or the Department of Health and Social Care.

Contributors Manuscript writing: CH, SK, XC and YZ. Data collection and image tracing: CH, MAh, MAi, AB, DM, TS, SR, AH, VR, GB, GC and SK. Artificial intelligence module training and testing: XC and YZ. Guarantor: SK.

Funding The authors have not declared a specific grant for this research from any funding agency in the public, commercial or not-for-profit sectors.

Competing interests SK, SR, VR and YZ are editors for *BMJ Open Ophthalmology*.

Patient and public involvement Patients and/or the public were not involved in the design, or conduct, or reporting, or dissemination plans of this research.

Patient consent for publication Not applicable.

Ethics approval Ethics approval was granted for this study by the North West—Liverpool Central Research Ethics Committee (reference number 18/NW/0760).

Provenance and peer review Not commissioned; internally peer reviewed.

Data availability statement Data are available on reasonable request. All data are available on request to the corresponding author.

ORCID iDs
Colby Hart https://orcid.org/0000-0002-3739-8177
Alfredo Borgia https://orcid.org/0000-0002-3976-242X
Tobi Somerville https://orcid.org/0009-0004-5662-5138
Vito Romano https://orcid.org/0000-0002-5148-7643
Gibran Butt https://orcid.org/0000-0001-5306-4647
Giulia Coco https://orcid.org/0000-0002-2410-6366
Yalin Zheng https://orcid.org/0000-0002-7873-0922

REFERENCES

1 Konstantopoulos A, Kuo J, Anderson D, *et al*. Assessment of the use of anterior segment optical coherence tomography in microbial keratitis. *Am J Ophthalmol* 2008;146:534–42.
2 Thormundsson B. AI corporate investment worldwide 2015-2021. 2022.
3 Yu KH, Beam AL, Kohane IS. Artificial intelligence in healthcare. *Nat Biomed Eng* 2018;2:719–31.
4 Jiang F, Jiang Y, Zhi H, *et al*. Artificial intelligence in healthcare: past, present and future. *Stroke Vasc Neurol* 2017;2:230–43.
5 Lee CS, Tyring AJ, Deruyter NP, *et al*. Deep-learning based, automated segmentation of macular edema in optical coherence tomography. *Biomed Opt Express* 2017;8:3440–8.
6 Abràmoff MD, Lou Y, Erginay A, *et al*. Improved Automated Detection of Diabetic Retinopathy on a Publicly Available Dataset Through Integration of Deep Learning. *Invest Ophthalmol Vis Sci* 2016;57:5200.
7 Li Z, He Y, Keel S, *et al*. Efficacy of a Deep Learning System for Detecting Glaucomatous Optic Neuropathy Based on Color Fundus Photographs. *Ophthalmology* 2018;125:1199–206.
8 Apushkin MA, Fishman GA, Janowicz MJ, *et al*. Bibliography Current World Literature. *Ophthalmology* 2005;111:2027–32.
9 Howard AG, Zhu M, Chen B, *et al*. Mobilenets: Efficient convolutional neural networks for mobile vision applications. *arXiv* 2017.
10 Soleimani M, Cheung AY, Rahdar A, *et al*. Diagnosis of microbial keratitis using smartphone-captured images; a deep-learning model. *J Ophthalmic Inflamm Infect* 2025;15:8.
11 Huang G, Liu Z, Van Der Maaten L, *et al*. Densely connected convolutional networks. 2017 IEEE Conference on Computer Vision and Pattern Recognition (CVPR).4700–8.
12 Wang L, Chen K, Wen H, *et al*. Feasibility assessment of infectious keratitis depicted on slit-lamp and smartphone photographs using deep learning. *Int J Med Inform* 2021;155:104583.
13 Polat H. A modified DeepLabV3+ based semantic segmentation of chest computed tomography images for COVID-19 lung infections. *Int J Imaging Syst Technol* 2022;32:1481–95.
14 Roy Choudhury A, Vanguri R, Jambawalikar SR, *et al*. Segmentation of brain tumors using deeplabv3+. Brainlesion: Glioma, Multiple Sclerosis, Stroke and Traumatic Brain Injuries: 4th International Workshop, BrainLes 2018, Held in Conjunction with MICCAI 2018, Revised Selected Papers, Part II 4 2019; Granada, Spain: Springer International Publishing, 2018:154–67.
15 Sorkhabi MA, Potapenko IO, Ilginis T, *et al*. Assessment of Anterior Uveitis Through Anterior-Segment Optical Coherence Tomography and Artificial Intelligence-Based Image Analyses. *Trans Vis Sci Tech* 2022;11:7.